*mathematics*

MDPI

*Article*

# A Partitioned IRS-Aided Transmit SM Scheme for Wireless Communication

**Liping Xiong [1,2], Yuyang Peng [1,*], Ming Yue [1], Haihong Wei [1], Runlong Ye [1], Fawaz AL-Hazemi [3] and Mohammad Meraj Mirza [4]**

[1] School of Computer Science and Engineering, Macau University of Science and Technology, Macau 999078, China; 2109853gii30012@student.must.edu.mo (L.X.); 2109853wii20001@student.must.edu.mo (M.Y.); 3220002301@student.must.edu.mo (H.W.); 3220002479@student.must.edu.mo (R.Y.)
[2] School of Electronic Information, Dongguan Polytechnic, Dongguan 523109, China
[3] Department of Computer and Network Engineering, University of Jeddah, Jeddah 21959, Saudi Arabia; fmalhazemi@uj.edu.sa
[4] Department of Computer Science, College of Computers and Information Technology, Taif University, Taif 21944, Saudi Arabia; mmmirza@tu.edu.sa
* Correspondence: yypeng@must.edu.mo

**Abstract:** In this paper, we present a practical partitioned intelligent-reflecting-surface-aided transmit spatial modulation (PIRS-TSM) scheme, where spatial modulation is implemented at the transmitter and partitioning is conducted on the IRS to enhance the spectral efficiency (SE) and reliability for multiple-input single-output (MISO) systems. The theoretical analysis of average bit error rate (ABER) based on maximum likelihood (ML) detection and the computational complexity analysis are provided. Experimental simulations demonstrate that the PIRS-TSM scheme obtains a significant ABER enhancement under the same SE compared to the existing partitioned IRS-aided transmit space shift keying or generalized space shift keying schemes by additionally carrying modulated symbols. Moreover, the system performances with different configurations of antenna numbers and symbol modulation orders under the same SE are investigated as a practical application reference.

**Keywords:** partitioned intelligent reflecting surface (PIRS); spatial modulation (SM); spectral efficiency (SE); average bit error rate (ABER)

**MSC:** 94-10

check for updates

Academic Editor: Jonathan Blackledge

Received: 18 February 2025
Revised: 21 April 2025
Accepted: 30 April 2025
Published: 2 May 2025

**Citation:** Xiong, L.; Peng, Y.; Yue, M.; Wei, H.; Ye, R.; AL-Hazemi, F.; Mirza, M.M. A Partitioned IRS-Aided Transmit SM Scheme for Wireless Communication. *Mathematics* **2025**, *13*, 1503. https://doi.org/10.3390/math13091503

**Copyright:** © 2025 by the authors. Licensee MDPI, Basel, Switzerland. This article is an open access article distributed under the terms and conditions of the Creative Commons Attribution (CC BY) license (https://creativecommons.org/licenses/by/4.0/).

## 1. Introduction

The six generation (6G) wireless communication requires significant innovation and progress of communication paradigm to meet the enormous demands for spectrum efficiency (SE) and energy efficiency (EE) [1,2]. Spatial modulation (SM) [3], essentially as a spatial multiplexing technology for wireless communication, has been emerging in recent years due to its high SE and EE. Unlike conventional signal transmission, SM conveys not only the modulated symbols, but also the index of the activated antenna as extra information. Moreover, inter-antenna synchronization (IAS) and inter-channel interference (ICI) are avoided due to the single-antenna activation. Later, SM was simplified as space shift keying (SSK) [4] in which only the activated antenna indices were conveyed to reduce the complexity of the system and detection. Furthermore, SM and SSK were respectively extended to generalized spatial modulation (GSM) [5] and generalized space shift keying

(GSSK) [6], where multiple antennas were activated simultaneously, thereby improving the diversity gain or SE for wireless communication systems.

On the other hand, intelligent reflecting surface (IRS), consisting of a large array of passive elements, is regarded as an intelligent device that can change electromagnetic waves by adjusting the phase of the incident signal, aiming to maximize the signal-to-noise ratio (SNR) of the receiver (Rx) [7,8]. Moreover, IRS signal reflection does not require a specialized RF chain for signal processing. Due to its advantages in high transmission reliability and EE, IRS is widely recognized as one of the most promising technologies for 6G [9].

In light of the significance of SM and IRS, exploring the potential of IRS-aided SM systems to achieve high reliability, SE, and EE, has been widely researched. Refs. [10–15] researched IRS-aided received SM or its evolution forms such as SSK, GSSK, and GSM in single-input multiple-output (SIMO) systems. The theoretical average bit error probability (ABER) and simulation analyses were provided, demonstrating the significant superiority of combining IRS and SM. Ref. [16] proposed IRS-assisted GSM with phase offset scheme, which enhanced the IRS beamforming and widened the activated antenna combination channel differences to improve the system bit error rate (BER) performance. Ref. [17] proposed a novel transmissive reconfigurable intelligent surface (TRIS) transmitter-enabled SM multiple-input multiple-output (MIMO) system where the specific column elements of the TRIS panel are activated per time slot.

Refs. [18–22] focused on the research of IRS-aided transmit SSK or GSSK in multiple-input single-output (MISO) systems. Moreover, IRS partitioning improved the distinctions between transmission channels and effectively improved the BER performance in the partitioned IRS-aided transmit SSK (PIRS-TSSK) scheme [20]. Then, it was extended to multi-antenna activated scenario and a partitioned IRS-aided transmit GSSK (PIRS-TGSSK) scheme and a partitioned IRS-aided flexible GSSK (PIRS-FGSSK) scheme were proposed to further improve SE and antenna utilization [22]. It is worth noting that although [22] improves antenna utilization compared to [20], it does not transmit symbols, which still limits the further enhancement of SE to some extent. In summary, in the existing studies mentioned above, the transmitter (Tx) employs SSK or GSSK, which only conveys antenna index information without carrying symbols. This can be considered as an absence of symbolic information transmission, which constrains the wireless communication system's SE. In particular, at high SE requirements, the number of transmit antennas required is large, thus leading to more groups of IRSs and fewer reflecting elements per group; then, the beamforming effect will deteriorate and the BER performance will decrease.

To address this issue, this paper proposes a partitioned IRS-aided transmit spatial modulation (PIRS-TSM) scheme. The contributions of this paper can be summarized as follows:

- In PIRS-TSM, SM is performed at the Tx, so both antenna index and modulated symbol can be transmitted in each time slot, effectively resolving the symbolic information absence issue inherent in [20,22]. In addition, the IRS is divided into groups corresponding to the transmit antennas and phase shifts are made on each IRS group corresponding to the transmit channel states to enhance the differences between channels so as to improve the BER performance. The proposed PIRS-TSM scheme achieves significantly better ABER performance compared to the unpartitioned IRS-TSM scheme. Moreover, even under the same partitioning strategy of IRS, the performance of PIRS-TSM is superior to the existing PIRS-TSSK [20], PIRS-TGSSK [22], and PIRS-FGSSK [22] schemes.
- The theoretical ABER bound of the proposed PIRS-TSM scheme is provided based on maximum likelihood (ML) detection and is confirmed by simulations. The computa-

tional complexity of the scheme is also investigated and compared with PIRS-TSSK and PIRS-TGSSK schemes.

- Compared with existing PIRS-TSSK, PIRS-TGSSK, and PIRS-FGSSK schemes, the joint transmission of antenna index and modulated symbol information and the configuration influence of antenna numbers and symbol orders of PIRS-TSM under the same SE have also been investigated in this paper. Simulation results show that the configuration with fewer transmit antennas and higher modulation orders has better BER performance.

The remainder of this paper is organized as follows. Section 2 details the proposed PIRS-TSM system model. Subsequently, Section 3 presents the theoretical derivation and analysis of PIRS-TSM ABER performance. Thereafter, Section 4 conducts an analysis and comparison of the computational complexity of ML detection. Section 5 provides the simulation results along with corresponding discussions and analyses. Finally, Section 6 concludes the paper by summarizing key contributions.

*Notation*: $X_{\Re}$ and $X_{\Im}$ represent the real and imaginary part of a complex variable $X$, respectively. $j = \sqrt{-1}$ represents the imaginary unit. E[$X$] and Var[X] denote the mean and variance of $X$, respectively.

## 2. System Model

### *2.1. Transmission*

The proposed PIRS-TSM system model is illustrated in Figure 1, where $N_t$ transmit antennas are deployed at the Tx and a single antenna is equipped at the Rx. In addition, an IRS is composed of $N$ reflecting elements which make phase shifts independently. Only one of the $N_t$ transmit antennas is activated to transmit information at each time. We follow the hypothesis that the information from Tx to Rx can be transmitted only through the IRS due to the physical barrier. Let vector $\boldsymbol{a} = [0 \quad 0 \ldots 1 \quad 0 \ldots 0]$ represent the transmit antennas, where only one non-zero element is used to represent the activated antenna. In contrast to the PIRS-TSSK system [20] where the incoming data bits exclusively map the activated antenna index, the PIRS-TSM system transmits both antenna index and modulated symbol. During each transmission time slot, the incoming data bits $S$ are divided into two parts: $S = S_1 + S_2$, in which $S_1 = \log_2 N_t$ bits denote the index of the activated antenna and $S_2 = \log_2 M$ bits denote the $M$-ary constellation symbols. Let $x$ represent the data symbol selected from $M$-ary constellations with normalized power, i.e., $|x|^2 = 1$.

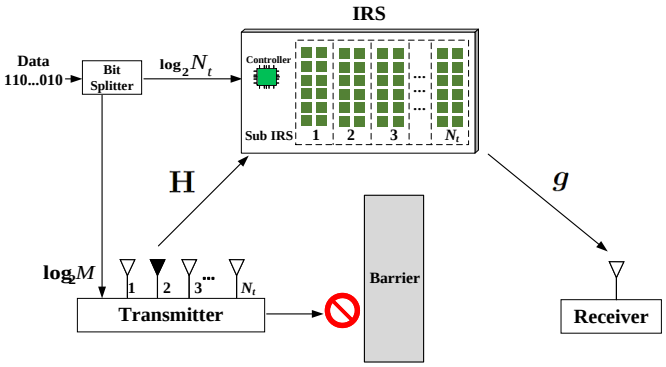



**Figure 1.** PIRS-TSM system model.

The channel from the Tx to the IRS is denoted by $\mathbf{H} \in \mathbb{C}^{N_t \times N}$, while the channel from the IRS to the Rx is denoted by $\boldsymbol{g} \in \mathbb{C}^{N \times 1}$. Assuming $\mathbf{H}$ and $\boldsymbol{g}$ follow independent Rayleigh fading $\mathcal{CN}(0,1)$, each entry of $\mathbf{H}$ is represented as $h_{t,i} = \alpha_{t,i} e^{-j\theta_{t,i}} (t = 1, \ldots, N_t, i = 1, \ldots, N)$, while each entry of $\boldsymbol{g}$ is represented as $g_i = \beta_i e^{-j\psi_i}$. The phase-shift matrix of the IRS is denoted by

a diagonal matrix $\mathbf{\Phi} \in \mathbb{C}^{N\times N}$, where each element represents the phase shift of a reflecting element, written as $e^{j\phi_i}(i = 1, \ldots, N)$. We assume perfect channel state information (CSI) at the Tx. The IRS obtains phase-shift information from the controller linked to the Tx.

In this system, the IRS partitioning method is the same as that of the PIRS-TSSK scheme, i.e., the IRS is divided into groups that have a one-to-one correspondence with the transmit antennas. Specifically, a total number of $N$ reflecting elements is divided into $N_t$ groups, each of which consists of $n = \frac{N}{N_t}$ elements. Each group of reflecting elements can be regarded as a sub-IRS, which maximizes the signal energy from the corresponding transmit antenna to the Rx by phase adjustment. Therefore, during data transmission of each time slot, no matter which transmit antenna is activated, all reflecting elements on the IRS work at predetermined phase-shift angles based on the CSI. In other words, all reflecting elements on the IRS work at the "ON" state, with one of the IRS groups able to fully offset the channel phases, while the other groups are not fully offset. In fact, this IRS partitioning method is a trade-off between widening the differences in the channels corresponding to different transmit antennas and maintaining the beamforming of the IRS. The partitioning method is validated to provide more diversity when activating different transmit antennas [22] so as to improve the BER performance. For convenience, the transmit energy is assumed to be 1, and the received signal can be expressed as follows:

$$y = \boldsymbol{a}\mathbf{H}\mathbf{\Phi}\boldsymbol{g}x + w = Lx + w, \tag{1}$$

where $w$ denotes the additive white Gaussian noise (AWGN) with mean 0 and variance $N_0$, and

$$L = \sum_{i=(t-1)n+1}^{tn} \alpha_{t,i}\beta_i + \sum_{\substack{k=1\\k\neq t}}^{N_t} \sum_{i=(k-1)n+1}^{kn} \alpha_{t,i}\beta_i e^{j\left(\theta_{k,i}-\theta_{t,i}\right)}, \tag{2}$$

with $k$ representing the index of the sub-IRS. The phase shift of the reflecting element on the $k$-th sub IRS is $\phi_{k,i} = \theta_{k,i} + \psi_i (k = 1, \ldots, N_t)$. When the $t$-th transmit antenna is activated, for the $k = t$ sub-IRS, the channel phases are completely canceled, while for the $k \neq t$ cases, the phases cannot be completely canceled.

### *2.2. Maximum Likelihood Detection*

A joint detection of antenna index $t$ and symbol $x$ based on the ML detector is utilized for our PIRS-TSM scheme, written as follows:

$$(\hat{t}, \hat{x}) = \underset{t,x}{\operatorname{argmin}} |y - Lx|^2, \tag{3}$$

where $\hat{t}$, $\hat{x}$ represent the estimated antenna index and symbol, respectively.

## 3. Performance Analysis

In this section, we make a theoretical analysis of the error performance for the PIRS-TSM scheme. The theoretical average pairwise error probability (APEP) for ML detection is derived, and then, the theoretical ABER can be obtained [23,24]. The conditional pairwise error probability (CPEP) with ML detection using (3) can be expressed as follows:

$$P_e(t, x \to \hat{t}, \hat{x})|\mathbf{H}, \boldsymbol{g}) = P\left\{|y - Lx|^2 > \left|y - \hat{L}\hat{x}\right|^2\right\}, \tag{4}$$

where

$$\hat{L} = \sum_{i=(\hat{t}-1)n+1}^{\hat{t}n} \alpha_{\hat{t},i}\beta_i + \sum_{\substack{k=1\\k\neq \hat{t}}}^{N_t} \sum_{i=(k-1)n+1}^{kn} \alpha_{\hat{t},i}\beta_i e^{j(\theta_{k,i}-\theta_{\hat{t},i})}. \tag{5}$$

After calculation, it can be concluded that

$$\begin{aligned} P_e &= P\Big\{ -\left|Lx - \hat{L}\hat{x}\right|^2 - 2[w^*(Lx - \hat{L}\hat{x})]_{\Re} > 0\Big\} \\ &= P\{\nu > 0\}, \end{aligned} \tag{6}$$

where $\nu = -\left|Lx - \hat{L}\hat{x}\right|^2 - 2[w^*(Lx - \hat{L}\hat{x})]_{\Re}$ with $w^*$ being the complex conjugate of $w$. It can be obtained that $\nu$ follows complex Gaussian distribution with mean $\mu_\nu$ and variance $\sigma_\nu^2$ since $w$ follows complex Gaussian distribution. We can calculate $\mu_\nu = -\left|Lx - \hat{L}\hat{x}\right|^2$, $\sigma_\nu^2 = 2N_0\left|Lx - \hat{L}\hat{x}\right|^2$. Let $B = Lx - \hat{L}\hat{x}$, using Gaussian $Q$-function, we have

$$P_e = Q\Big(\sqrt{\frac{|B|^2}{2N_0}}\Big). \tag{7}$$

Assuming $\lambda = |B|^2$, the APEP can be obtained as follows:

$$\begin{aligned} \bar{P}_e &= \int_0^\infty Q\Big(\sqrt{\frac{\lambda}{2N_0}}\Big) f_\lambda(\lambda) d\lambda \\ &= \frac{1}{\pi}\int_0^{\frac{\pi}{2}} M_\lambda\Big(\frac{-1}{4N_0 \sin^2\eta}\Big) d\eta, \end{aligned} \tag{8}$$

where $f_\lambda(\lambda)$ and $M_\lambda(s)$ are the probability density function (PDF) and moment-generating function (MGF) of $\lambda$, respectively. Then, we will discuss the distribution of $\lambda$ in different cases to obtain the corresponding MGF. In (7), it can be easily written that $|B|^2 = B_{\Re}^2 + B_{\Im}^2$.

*(1) First case* ($t = \hat{t}$): Assume that the activated antenna index is correctly detected. We have $B = L(x - \hat{x})$. Then, we obtain

$$\lambda = |B|^2 = |L|^2 \cdot |x - \hat{x}|^2 = \left(L_{\Re}^2 + L_{\Im}^2\right)|x - \hat{x}|^2, \tag{9}$$

where

$$L_{\Re} = \sum_{i=(t-1)n+1}^{tn} \alpha_{t,i}\beta_i + \sum_{\substack{k=1 \\ k\neq t}}^{N_t} \sum_{i=(k-1)n+1}^{kn} \left(\alpha_{t,i}\beta_i e^{j\left(\theta_{k,i} - \theta_{t,i}\right)}\right)_{\Re},$$

$$L_{\Im} = \sum_{\substack{k=1 \\ k\neq t}}^{N_t} \sum_{i=(k-1)n+1}^{kn} \left(\alpha_{t,i}\beta_i e^{j\left(\theta_{k,i} - \theta_{t,i}\right)}\right)_{\Im}.$$

Next, we will analyze the distribution of $\lambda$, and then obtain the MGF based on its distribution. In order to analyze the distribution of $\lambda$, we need to express $\lambda$ as the sum of two components, i.e., $\lambda = \lambda_1 + \lambda_2$, where $\lambda_1 = L_{\Re}^2|x - \hat{x}|^2$, $\lambda_2 = L_{\Im}^2|x - \hat{x}|^2$. Then, the MGF satisfies the following relationship:

$$M_\lambda(s) = M_{\lambda_1}(s) \cdot M_{\lambda_2}(s). \tag{10}$$

It is known that $\beta_i$ and $\alpha_{t,i}$ are independent and follow Rayleigh distribution with mean $\frac{\sqrt{\pi}}{2}$ and variance $\frac{4-\pi}{4}$. We consider the characteristics of mean and variance between independent random variable (RV)s and utilize the relevant derivations. Specifically, for the independent RVs $X$ and $Y$, the mean and variance follow the rules: $\mathrm{E}[XY] = \mathrm{E}[X]\mathrm{E}[Y]$, $\mathrm{Var}[XY] = \mathrm{Var}[X]\mathrm{Var}[Y] + \mathrm{E}^2[X]\mathrm{Var}[Y] + \mathrm{E}^2[Y]\mathrm{Var}[X]$, $\mathrm{E}[X + Y] = \mathrm{E}[X] + \mathrm{E}[Y]$, $\mathrm{Var}[X \pm Y] = \mathrm{Var}[X] + \mathrm{Var}[Y]$, while for the un-independent RVs $X$ and $Y$, the

property of covariance is $\mathrm{Cov}(X,Y) = \frac{1}{2}(\mathrm{Var}[X+Y] - \mathrm{Var}[X] - \mathrm{Var}[Y])$. Then the mean and variance of the following terms can be figured out as follows:

$$\mathrm{E}[\alpha_{t,i}\beta_i] = \frac{\pi}{4},$$

$$\mathrm{Var}[\alpha_{t,i}\beta_i] = \frac{16-\pi^2}{16},$$

$$\mathrm{E}[\left(\alpha_{t,i}\beta_i e^{j\left(\theta_{k,i}-\theta_{t,i}\right)}\right)_{\Re}] = \mathrm{E}[\left(\alpha_{t,i}\beta_i e^{j\left(\theta_{k,i}-\theta_{t,i}\right)}\right)_{\Im}] = 0,$$

$$\mathrm{Var}[\left(\alpha_{t,i}\beta_i e^{j\left(\theta_{k,i}-\theta_{t,i}\right)}\right)_{\Re}] = \mathrm{Var}[\left(\alpha_{t,i}\beta_i e^{j\left(\theta_{k,i}-\theta_{t,i}\right)}\right)_{\Im}] = \frac{1}{2}.$$

After some mathematical calculations, we have $\mathrm{E}[L_{\Re}] = \frac{n\pi}{4}$, $\mathrm{Var}[L_{\Re}] = \frac{n(16-\pi^2+8N_t-8)}{16}$. It can be seen that $\lambda_1 = L_{\Re}^2|x-\hat{x}|^2$ is a non-central chi-square RV with one degree of freedom. Since the number of reflecting elements $N \gg 1$, the Central Limit Theorem (CLT) is applicable. Assuming $\mu_r = \mathrm{E}[L_{\Re}], \sigma_r^2 = \mathrm{Var}[L_{\Re}]$, according to the genetic characteristic function (CF) of the non-central $\chi^2$ distribution, the MGF of $\lambda_1$ can be obtained as follows [5]:

$$M_{\lambda_1}(s) = \left(\frac{1}{1-2s\sigma_r^2|x-\hat{x}|^2}\right)^{\frac{1}{2}} \exp\left(\frac{s\mu_r^2|x-\hat{x}|^2}{1-2s\sigma_r^2|x-\hat{x}|^2}\right). \tag{11}$$

Similarly, it can be calculated that $\mathrm{E}[L_{\Im}] = 0$, and $\sigma_l^2 = \mathrm{Var}[L_{\Im}] = \frac{n(N_t-1)}{2}$. Therefore, $\lambda_2 = L_{\Im}^2|x-\hat{x}|^2$ is a central chi-square RV with one degree of freedom. The MGF of $\lambda_2$ can be obtained as follows:

$$M_{\lambda_2}(s) = \left(\frac{1}{1-2s\sigma_l^2|x-\hat{x}|^2}\right)^{\frac{1}{2}}. \tag{12}$$

Then, the MGF of $\lambda$ can be obtained by substituting (11) and (12) to (10). Finally, substitute the MGF of $\lambda$ to Equation (8) to calculate APEP. It is worth noting that the APEP is independent of $t$ and $\hat{t}$.

*(2) Second case* ($t \neq \hat{t}$): Assume that the antenna index is detected erroneously. Then, we have $B = Lx - \hat{L}\hat{x}$. Consequently, we have

$$\lambda = |B|^2 = |Lx - \hat{L}\hat{x}|^2 = B_{\Re}^2 + B_{\Im}^2, \tag{13}$$

while $B_{\Re} \sim \mathcal{N}\left(\mu_{B_{\Re}}, \sigma_{B_{\Re}}^2\right)$ and $B_{\Im} \sim \mathcal{N}\left(\mu_{B_{\Im}}, \sigma_{B_{\Im}}^2\right)$, respectively. The next step is to analyze the distribution of $B_{\Re}$ and $B_{\Im}$ and their relevance. We rewrite $x$ and $\hat{x}$ in the form of adding the real and imaginary parts: $x = x_{\Re} + jx_{\Im}, \hat{x} = \hat{x}_{\Re} + j\hat{x}_{\Im}$. Then, we have

$$B_{\Re} = \left[L(x_{\Re} + jx_{\Im}) - \hat{L}(\hat{x}_{\Re} + j\hat{x}_{\Im})\right]_{\Re}, \tag{14}$$

$$B_{\Im} = \left[L(x_{\Re} + jx_{\Im}) - \hat{L}(\hat{x}_{\Re} + j\hat{x}_{\Im})\right]_{\Im}. \tag{15}$$

Then, substituting $L$ and $\hat{L}$ as Equations (2) and (5) into Equations (14) and (15), respectively, and after a series of tedious calculations, the mean vector and covariance matrix of $\mathbf{b} = [B_{\Re}, B_{\Im}]^{\mathrm{T}}$ can be obtained as follows:

$$\boldsymbol{\mu} = [\mu_1, \mu_2]^{\mathrm{T}}, \tag{16}$$

$$\mathbf{C} = \begin{bmatrix} \sigma_1^2 & \sigma_{1,2} \\ \sigma_{1,2} & \sigma_2^2 \end{bmatrix}, \tag{17}$$

where

$$\begin{aligned} \mu_1 &= \frac{n\pi(x_{\Re} - \hat{x}_{\Re})}{4}, \mu_2 = \frac{n\pi(x_{\Im} - \hat{x}_{\Im})}{4}, \\ \sigma_1^2 &= \frac{n(N_t - 1)(|x|^2 + |\hat{x}|^2)}{2} + \frac{n(16 - \pi^2)(x_{\Re}^2 + \hat{x}_{\Re}^2)}{16}, \\ \sigma_2^2 &= \frac{n(N_t - 1)(|x|^2 + |\hat{x}|^2)}{2} + \frac{n(16 - \pi^2)(x_{\Im}^2 + \hat{x}_{\Im}^2)}{16}. \end{aligned}$$

Next, according to the property of the covariance, we figure out the covariance of $B_{\Re}$ and $B_{\Im}$ as follows:

$$\sigma_{1,2} = \frac{n(16 - \pi^2)(x_{\Re}x_{\Im} + \hat{x}_{\Re}\hat{x}_{\Im})}{16}. \tag{18}$$

Furthermore, we utilize the MGF of the generalized non-central chi-square distribution as follows [23]:

$$\begin{aligned} M_X(s) = &[\det(\mathbf{I} - 2s\mathbf{C})]^{-\frac{1}{2}} \\ &\times \exp\left(-\frac{1}{2}\boldsymbol{\mu}^{\mathrm{T}}\left[\mathbf{I} - (\mathbf{I} - 2s\mathbf{C})^{-1}\right]\mathbf{C}^{-1}\boldsymbol{\mu}\right), \end{aligned} \tag{19}$$

where $X = X_1^2 + X_2^2 + \cdots + X_n^2$, $\mathbf{I}$ is the unit matrix, and $\boldsymbol{\mu}$ and $\mathbf{C}$ are the mean and covariance matrix of $[X_1^2, X_2^2, \ldots, X_n^2]^{\mathrm{T}}$, respectively. Substituting Equations (16) and (17) to Equation (19), we can obtain the MGF of $\lambda$ in the case of $t \neq \hat{t}$. Then, substitute Equation (19) to Equation (8) to calculate APEP. Further, the theoretical ABER can be derived based on the union bound technique by substituting APEP into the following equation:

$$\bar{P}_b = \frac{1}{N_t M}\sum_{t}\sum_{\hat{t}}\sum_{x}\sum_{\hat{x}}\frac{e(t, x \to \hat{t}, \hat{x})\bar{P}_e(t, x \to \hat{t}, \hat{x})}{\log_2 N_t M}, \tag{20}$$

where $e(t, x \to \hat{t}, \hat{x})$ denotes the number of bits in error for the corresponding pairwise error event.

## 4. Detection Complexity Analysis

In this section, we compare the computational complexity of PIRS-TSSK, PIRS-TGSSK, and the proposed PIRS-TSM scheme during ML detection, as shown in Table 1. In addition, we make a detection complexity analysis of the PIRS-TSM scheme with different numbers of transmit antennas $N_t$ and modulation orders $M$ at the same SE. The computational complexity is investigated with the number of real multiplications (RMs) and real additions (RAs) in ML detection. First, for the PIRS-TSSK scheme, the computational complexity is derived from the expression of ML detection ([20], Equation (14)). There is one group of reflecting elements that completely cancel out the channel phases, resulting in $\frac{N}{N_t}$ RM terms: $\alpha_{t,i}\beta_i$. Meanwhile, the remaining $(N_t - 1)$ groups of reflecting elements cannot completely cancel out the channel phases, resulting in $(N_t - 1)\frac{N}{N_t}$ multiplications of three complex numbers: $h_{t,i}e^{j\phi_{k,i}}g_i$, each of which requires eight RMs and four RAs. Similarly, the computational complexity of PIRS-TGSSK is analyzed from the ML detection expression ([22], Equation (3)). In GSSK here, we asume that $C = 2^a$ combinations are utilized, with defining $a = \left\lfloor \log_2 \binom{N_t}{N_s} \right\rfloor$, SE $= a$ bit/s/Hz.

On the other hand, the computational complexity of the proposed PIRS-TSM scheme is derived from the ML detection expression Equation (3), which has an additional product term of complex number $x$, resulting in an added complex multiplication for each reflecting element. Then, it can be obtained that each of the reflecting element that perfectly cancels out the channel phases requires three RMs, while each of the remaining reflecting elements

that cannot completely cancel out the channel phases requires four complex multiplications, each of which requires twelve RMs and six RAs.

**Table 1.** Detection complexity analysis summary.

| Scheme | RMs | RAs |
|---|---|---|
| PIRS-TSSK | $(8N - \frac{7N}{N_t} + 3)N_t$ | $(6N - \frac{5N}{N_t})N_t$ |
| PIRS-TGSSK | $(8N - \frac{7N}{N_t} + 4)N_t$ | $(6N - \frac{5N}{N_t})N_t + C$ |
| PIRS-TSM | $(12N - \frac{9N}{N_t} + 2)N_tM$ | $(8N - \frac{7N}{N_t})N_tM$ |

Table 1 summarizes the RMx and RA formulas for the PIRS-TSSK, PIRS-TGSSK, and PIRS-TSM schemes, demonstrating that the computational complexity primarily depends on the values of $N_t$ and $M$ under the same number of reflecting elements $N$. Moreover, a computational complexity comparison bar is provided in Figure 2 for an example of SE = 4 bit/s/Hz and $N = 128$. The PIRS-TSM scheme is configured as three scenarios: $N_t = 8, M = 2$; $N_t = 4, M = 4$; and $N_t = 2, M = 8$. The computational complexity of PIRS-TGSSK is lower than that of PIRS-TSSK under the same SE because PIRS-TGSSK requires fewer $N_t$. Among the three configuration scenarios of PIRS-TSM (the three green bars), the configuration with $N_t$ = 2 and $M$ = 8 has the lowest computational complexity. It can be seen that under the same SE, when $N_t$ is smaller and $M$ is larger, the computational complexity of PIRS-TSM is lower. This is because fewer transmit antennas implies fewer partitions on the IRS, resulting in lower computational complexity. When compared with PIRS-TSSK, PIRS-TSM with the configuration of $N_t = 2$ and $M = 8$ has a lower computational complexity. However, the computational complexities of the configurations with $N_t = 4$ and $M = 4$, and $N_t = 8$ and $M = 2$, are both higher than that of PIRS-TSSK. It is worth mentioning that the BER performance of PIRS-TSM with $N_t = 2$ and $M = 8$ is also optimal, which will be illustrated in the next section.

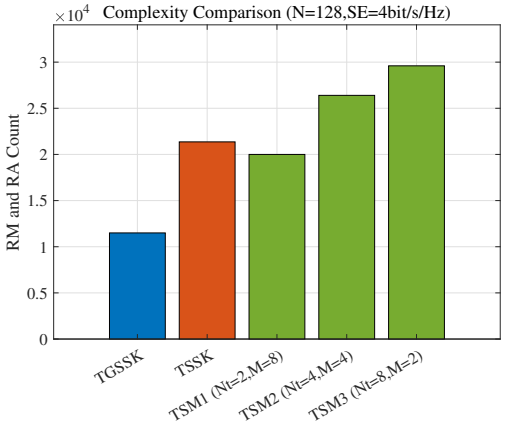



**Figure 2.** Comparison of computational complexity between PIRS-TGSSK, PIRS-TSSK, and PIRS-TSM (N = 128, SE = 4 bit/s/Hz).

## 5. Simulation Results

In this section, the analytical and numerical results of the BER performance of the proposed PIRS-TSM scheme with different system configurations are demonstrated through Monte Carlo simulations. Furthermore, the comparisons among the proposed PIRS-TSM, unpartitioned IRS-aided transmit SM (IRS-TSM), PIRS-TSSK [20], PIRS-TGSSK [22], and PIRS-FGSSK [22] schemes are conducted to demonstrate the effectiveness of IRS partitioning and symbols carrying in enhancing system performances. To ensure fair performance comparisons, this study evaluates the BER of different schemes under the same SE. Meanwhile, in order to facilitate the configuration of $N_t$ and $M$ under the same SE and evaluate

the impact of different SM configurations on PIRS-TSM system performance, we adopt SE = 4 bit/s/Hz for simulations. The system performances are compared by the SNR values (X-axis) of schemes at a certain BER value (Y-axis).

Figure 3 shows the simulated and theoretical BER performance for various values of $N$ (64, 128, 256), with the configuration of $N_t = 2$ and $M = 8$ and $N_t = 8$ and $M = 2$, respectively. As seen in Figure 3, as the number of reflecting elements increases, the BER performance of the system is superior, demonstrating the improvement of the channel propagation environment caused by the phase shift of IRS. Moreover, the theoretical results are very close to the experimental results in the area of high SNR. For the same N, the BER performance of the configuration with $N_t = 2$ and $M = 8$ outperforms that of $N_t = 8$ and $M = 2$, and its theoretical results show closer agreement with experimental data in the low-SNR region.

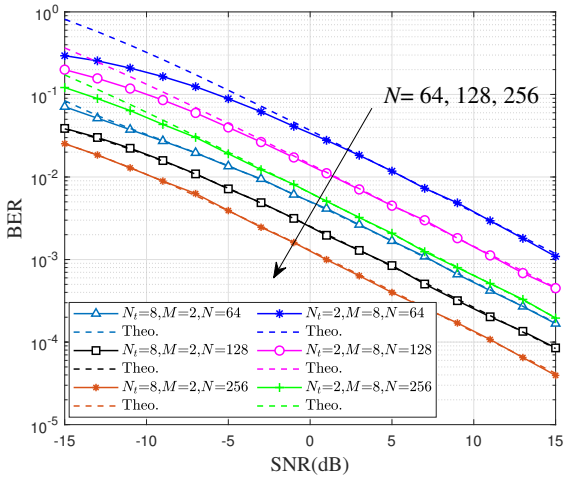



**Figure 3.** Theoretical and computer simulation results for PIRS-TSM with different $N$ when SE is 4 bit/s/Hz ($N_t = 2, M = 8$ and $N_t = 8, M = 2$).

Figure 4 demonstrates the agreement between theoretical and experimental BER performance at two SE examples. First, SE = 4 bit/s/Hz with configurations $N_t = 8$ and $M = 2$; $N_t = 4$ and $M = 4$; and $N_t = 2$ and $M = 8$. Second, SE = 6 bit/s/Hz with configurations $N_t = 8$ and $M = 8$; $N_t = 4$ and $M = 16$; and $N_t = 2$ and $M = 32$. The legend parameters are set in the format (SE, $N_t$, $M$). It can be seen that the theoretical results fit the simulation results very closely. In addition, lower $N_t$ with higher $M$ configurations (e.g., (4, 2, 8) (6, 2, 32) vs. (4, 8, 2)(6, 8, 8)) achieve superior BER performance. The reason is that only one group of reflecting elements completely cancels out the channel phases in our IRS partitioning method. Therefore, with the same total number of reflecting elements, the more transmit antennas there are, the more groups are divided on the IRS, and the fewer reflecting elements each group has, leading to some degradation of the IRS beamforming. Quantitatively, as seen in Figure 4, when BER = $10^{-3}$, PIRS-TSM at SE = 4 bit/s/Hz with $N_t = 2, M = 8$ contributes approximately 2.5 dB SNR gain over $N_t = 4, M = 4$ and 7.5 dB SNR gain over $N_t = 8, M = 2$. When BER = $10^{-2}$ and SE is 6 bit/s/Hz, PIRS-TSM with $N_t = 2, M = 32$ obtains about 7.5 dB SNR gain over $N_t = 4, M = 16$ and 14.5 dB SNR gain over $N_t = 8, M = 8$. This shows that as the SE increases, the PIRS-TSM in the configuration with fewer antennas exhibits a more pronounced performance advantage.

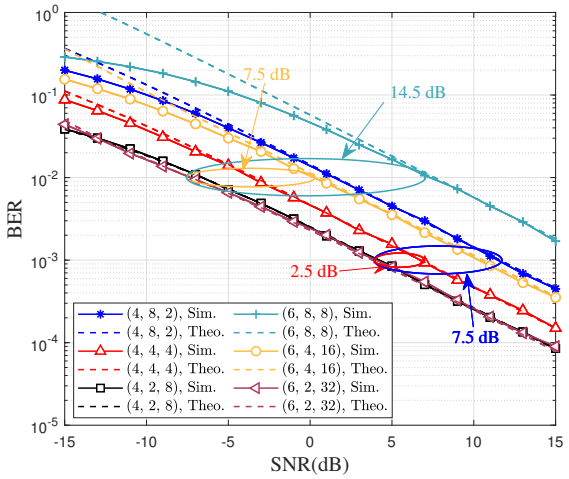



**Figure 4.** Theoretical and computer simulation results for PIRS-TSM with 3 different configurations when SE is 4 bit/s/Hz and 6 bit/s/Hz, respectively.

In Figure 5, the effect of partitioning on the IRS is illustrated by making a BER performance comparison between PIRS-TSM and unpartitioned IRS-TSM in the above 3 configurations, respectively. Specifically, in the IRS-TSM scheme, during each transmission, all IRS reflecting elements work at phase shifs to cancel the channel phases from the activated antenna to the IRS then to the Rx in order to maximize the SNR at the Rx. We can observe that the reliability of signal transmission is significantly improved by partitioning on the IRS, especially at high SNR. Taking the scenario of $N_t = 2, M = 8$ as an example. Select the points of PIRS-TSM at $-11$ dB and $-1$ dB as the low-SNR and high-SNR comparison points, respectively. To match the BER performance of PIRS-TSM at $-11$ dB, the IRS-TSM scheme requires an approximate 8.5 dB SNR gain. Notably, this performance gap widens significantly in the high-SNR region, where IRS-TSM demands a 16 dB SNR gain to achieve the same BER as PIRS-TSM at $-1$ dB. This trend highlights the enhanced effectiveness of PIRS-TSM in high-SNR scenarios, attributed to its optimized IRS partitioning and phase alignment mechanisms.

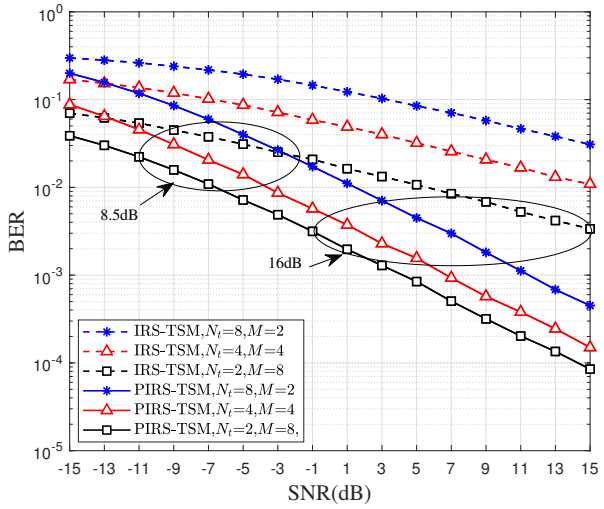



**Figure 5.** Performance comparison between PIRS-TSM and IRS-TSM with 3 different configurations when SE is 4 bit/s/Hz.

Figure 6 investigates the effect of carrying symbols on the transmission performance of the system with the same IRS partitioning method, by making a comparison of the BER

performance among the PIRS-TSM, PIRS-TSSK, PIRS-TGSSK, and PIRS-FGSSK schemes. The system parameters are still uniformly configured as SE $=$ 4 bit/s/Hz, $N = 128$. The performance curves of the proposed PIRS-TSM scheme for the three aforementioned configurations are given. For the required SE of 4 bit/s/Hz, the number of transmit antennas for PIRS-TSSK should be $N_t = 16$, and the PIRS-TGSSK scheme needs 7 transmit antennas and 2 activated antennas. The number of transmit antennas for the PIRS-FGSSK scheme, which has a flexible number of activated antennas, is set as $N_t = 8$. The reasons for chosing the number of transmit antennas in these schemes are as follows: for PIRS-TSSK, SE = $\log N_t$, so $N_t$ is set as 16 to achieve an SE of 4 bits/s/Hz. For PIRS-TGSSK, the number of possible transmit antenna combinations is $\binom{N_t}{N_s}$ with $N_s$ denoting the number of activated antennas. Because the number of activated antenna combinations must be a power of 2, $C = 2^a$ combinations are utilized, with SE = $a = \left\lfloor \log_2 \binom{N_t}{N_s} \right\rfloor$ bit/s/Hz. Therefore, $N_t = 7$ and $N_s = 2$ can achieve an SE of 4 bits/s/Hz. For PIRS-FGSSK, the number of activated antennas is flexible, we set $N_t = 8$ to achieve an SE of 4 bits/s/Hz. It can be seen that the BER performance of the PIRS-TSM scheme is superior to the other three schemes. For example, when BER $= 10^{-2}$, PIRS-TSM with $N_t = 2$ and $M = 8$ achieves about 14 dB, 12 dB, and 8 dB SNR gain compared with PIRS-TGSSK, PIRS-TSSK, and PIRS-FGSSK, respectively.

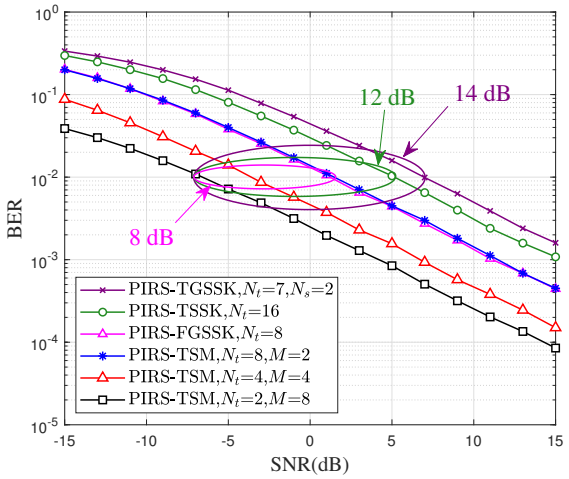



**Figure 6.** Performance comparison among PIRS-TSM, PIRS-TSSK, PIRS-TGSSK, and PIRS-FGSSK when SE is 4 bit/s/Hz.

## 6. Conclusions

In this paper, a PIRS-TSM scheme is proposed and efficiently improves the reliability and SE of the wireless system. The utilization of IRS partitioning improves the BER performance for antenna-indexed data bit transmission. In addition, both antenna index and modulated symbol transmission improve the SE of the system and achieve configurability between the number of transmit antennas and symbol modulation order, resulting in better performance than PIRS-TSSK or PIRS-TGSSK. Simulations also indicate that under the same SE, the BER performance is better and the computational complexity is lower when fewer transmit antennas and higher symbol modulation orders are set in PIRS-TSM.

**Author Contributions:** Conceptualization, L.X. and Y.P.; methodology, L.X.; validation, L.X.; formal analysis, L.X.; investigation, L.X.; writing—original draft preparation, L.X. and Y.P.; writing—review and editing, M.Y., H.W., R.Y., F.A.-H., M.M.M. and Y.P.; visualization, L.X.; supervision, Y.P.; project administration, Y.P.; funding acquisition, Y.P. All authors have read and agreed to the published version of the manuscript.

**Funding:** This work was supported by the Science and Technology Development Fund, Macau, SAR (0085/2024/RIA2), Dongguan Polytechnic National Double High Program Electronic Information Engineering Technology Fund (ZXF004), and the Scientific Research Projects of Department of Education of GuangDong Province (No. 2023KCXTD082). Also, this research was funded by Taif University, Saudi Arabia, Project No. (TU-DSPP-2025-71).

**Data Availability Statement:** The original contributions presented in this study are included in the article. Further inquiries can be directed to the corresponding author.

**Acknowledgments:** The authors extend their appreciation to Taif University, Saudi Arabia, for supporting this work through project number (TU-DSPP-2025-71).

**Conflicts of Interest:** The authors declare no conflicts of interest.

## References

1. Giordani, M.; Polese, M.; Mezzavilla, M.; Rangan, S.; Zorzi, M. Toward 6G networks: Use Cases and Technologies. *IEEE Commun. Mag.* **2020**, *58*, 55–61. [CrossRef]
2. Jiang, W.; Han, B.; Habibi, M.A.; Schotten, H.D. The road towards 6G: A comprehensive survey. *IEEE Open J. Commun. Soc.* **2021**, *2*, 334–366. [CrossRef]
3. Mesleh, R.Y.; Haas, H.; Sinanovic, S.; Ahn, C.W.; Yun, S. Spatial modulation. *IEEE Trans. Veh. Technol.* **2008**, *57*, 2228–2241. [CrossRef]
4. Jeganathan, J.; Ghrayeb, A.; Szczecinski, L.; Ceron, A. Space shift keying modulation for MIMO channels. *IEEE Trans. Wirel. Commun.* **2009**, *8*, 3692–3703. [CrossRef]
5. Younis, A.; Serafimovski, N.; Mesleh, R.; Haas, H. Generalised spatial modulation. In Proceedings of the 2010 Conference Record of the Forty Fourth Asilomar Conference on Signals, Systems and Computers, IEEE, Pacific Grove, CA, USA, 7–10 November 2010; pp. 1498–1502.
6. Jeganathan, J.; Ghrayeb, A.; Szczecinski, L. Generalized space shift keying modulation for MIMO channels. In Proceedings of the 2008 IEEE 19th International Symposium on Personal, Indoor and Mobile Radio Communications, Cannes, France, 15–18 September 2008; pp. 1–5.
7. Wu, Q.; Zhang, S.; Zheng, B.; You, C.; Zhang, R. Intelligent reflecting surface-aided wireless communications: A tutorial. *IEEE Trans. Commun.* **2021**, *69*, 3313–3351. [CrossRef]
8. ElMossallamy, M.A.; Zhang, H.; Song, L.; Seddik, K.G.; Han, Z.; Li, G.Y. Reconfigurable intelligent surfaces for wireless communications: Principles, challenges, and opportunities. *IEEE Trans. Cogn. Commun. Netw.* **2020**, *6*, 990–1002. [CrossRef]
9. Zhang, Z.; Xiao, Y.; Ma, Z.; Xiao, M.; Ding, Z.; Lei, X.; Karagiannidis, G.K.; Fan, P. 6G wireless networks: Vision, requirements, architecture, and key technologies. *IEEE Veh. Technol. Mag.* **2019**, *14*, 28–41. [CrossRef]
10. Basar, E. Reconfigurable intelligent surface-based index modulation: A new beyond MIMO paradigm for 6G. *IEEE Trans. Commun.* **2020**, *68*, 3187–3196. [CrossRef]
11. Zhang, C.; Peng, Y.; Li, J.; Tong, F. An IRS-aided GSSK scheme for wireless communication system. *IEEE Commun. Lett.* **2022**, *26*, 1398–1402. [CrossRef]
12. Zhang, L.; Lei, X.; Xiao, Y.; Ma, T. Large intelligent surface-based generalized index modulation. *IEEE Commun. Lett.* **2021**, *25*, 3965–3969. [CrossRef]
13. Li, C.; Cai, X.; Kang, P.; Chen, P. Exploiting activation mode index for reconfigurable intelligent surface-aided spatial modulation. *IEEE Trans. Veh. Technol.* **2024**, *73*, 19809–19814. [CrossRef]
14. Jin, X.; Li, X.; Feng, Y.; Wen, M.; Yao, Y. Joint RIS grouping design assisted generalized quadrature reflection modulation. *IEEE Trans. Veh. Technol.* **2023**, *72*, 5447–5451. [CrossRef]
15. Marn, P.A.; Hanif, M.; Bedeer, E. RIS-assisted receive generalized space shift keying and receive generalized spatial modulation. *IEEE Wirel. Commun. Lett.* **2024**, *13*, 2712–2716. [CrossRef]
16. Zhang, L.; Xiao, Y.; Lei, X.; Ma, T.; Xiang, W. Reconfigurable intelligent surface-assisted generalized spatial modulation with phase offset: Efficient designs for single-RF MIMO systems. *IEEE Trans. Veh. Technol.* **2024**, *73*, 15239–15254. [CrossRef]
17. Zhu, X.; Wu, Q.; Chen, W. Transmissive RIS transmitter enabled spatial modulation MIMO systems. *IEEE J. Sel. Areas Commun.* **2025**, *43*, 899–911. [CrossRef]
18. Canbilen, A.E.; Basar, E.; Ikki, S.S. Reconfigurable intelligent surface-assisted space shift keying. *IEEE Wirel. Commun. Lett.* **2020**, *9*, 1495–1499. [CrossRef]
19. Li, Q.; Wen, M.; Wang, S.; Alexandropoulos, G.C.; Wu, Y.-C. Space shift keying with reconfigurable intelligent surfaces: Phase configuration designs and performance analysis. *IEEE Open J. Commun. Soc.* **2021**, *2*, 322–333. [CrossRef]

20. Canbilen, A.E.; Basar, E.; Ikki, S.S. On the performance of RIS-assisted space shift keying: Ideal and non-ideal transceivers. *IEEE Trans. Commun.* **2022**, *70*, 5799–5810. [CrossRef]
21. Yue, M.; Peng, Y.; Lee, J. RIS-assisted flexible space shift keying for wireless communication system. *IEEE Wirel. Commun. Lett.* **2023**, *12*, 1776–1780. [CrossRef]
22. Xiong, L.; Peng, Y.; Lee, J. A partitioned-IRS assisted transmit GSSK scheme for wireless communication system. *IEEE Wirel. Commun. Lett.* **2024**, *13*, 260–264. [CrossRef]
23. Mathai, A.; Provost, S.B. *Quadratic Forms in Random Variables: Theory and Applications*; Marcel Dekker: New York, NY, USA, 1992.
24. Basar, E.; Aygolu, U.; Panayirci, E.; Poor, H.V. Performance of spatial modulation in the presence of channel estimation errors. *IEEE Commun. Lett.* **2012**, *16*, 176–179. [CrossRef]

**Disclaimer/Publisher's Note:** The statements, opinions and data contained in all publications are solely those of the individual author(s) and contributor(s) and not of MDPI and/or the editor(s). MDPI and/or the editor(s) disclaim responsibility for any injury to people or property resulting from any ideas, methods, instructions or products referred to in the content.